Title
A Luenberger Observer-Based Fault Detection and Identification Scheme for Photovoltaic DC-DC Converters

Author
Palak, Jain

Publication Date
2017-12-18

A Luenberger Observer-Based Fault Detection and Identification Scheme for Photovoltaic DC-DC Converters

Palak Jain*, Li Jian†, Jason Poon‡, Costas Spanos‡, Seth R. Sanders‡,
Jian-Xin Xu*, and Sanjib Kumar Panda*

*ECE Department, National University of Singapore
†School of Automation Engineering, Northeast Electric Power University, China
‡Department of EECS, University of California, Berkeley

***Abstract*—This paper presents the design, analysis, and experimental validation of a fault detection and identification (FDI) scheme for dc-dc power electronic converters. The FDI scheme includes two new classes of fault filters: (1) a linear-switched fault detection (FD) filter and (2) a bank of linear-switched fault identification (FI) filters. Both the FD filter and the bank of FI filters have a structure similar to that of Luenberger observer. The FD filter detects a fault event and the bank of FI filters identify a faulted converter component, for instance, failure in switching or passive components. We present simulation and experimental results for a prototype 2 kW solar photovoltaic (PV) boost dc-dc converter system to demonstrate the efficacy of the proposed FDI scheme. The experimental results demonstrate accurate fault detection and identification for a collection of catastrophic component faults in PV dc-dc power converters.**

***Index Terms*—Fault detection, fault diagnosis, fault location, converters, state estimation, photovoltaic (PV) systems**

I. Introduction

The dc power electronic systems are increasingly becoming complex and their applications in mission-critical- and safety-systems (e.g. avionics, space-transport, electric vehicles), information and communication systems (e.g. data centres), renewable energy technologies (e.g. photovoltaics systems), zero-energy buidings and intergrid [1] require a high level of dependability and reliabilty [2], [3]. For instance, converter component faults may degrade system performance and endanger safety and security of system operation. Thus, it is necessary, in many cases, to quickly detect and accurately identify the location of any fault in these systems. This is the purpose of fault detection and identification (FDI) scheme whose design becomes a mandatory complement to the system design process. In general, FDI schemes fall into two broad categories: model-based or model-free [4].

Model-based FDI schemes leverage analytical redundancy which includes signal processing techniques, state estimators (e.g. Luenberger observers and Kalman filters), parity space methods, and parameter estimation [5]. These FDI schemes have been investigated in the literature before [4], [6]–[11] for dc-dc converters. However, most of the earlier works are fault-specific, for instance in [6], [7] only switch faults are investigated using signal processing techniques for dc-dc converters.

Few works have focused on a generalized model-based methodologies for fault prognosis and diagnosis which are converter topology- and fault-agnostic [4], [10], [11]. However, the FDI schemes based on parity space methods in [4], [10] lack design for robustness, and are limited in identifying faults (for instance, the fault signatures used to identify different faults are indistinguishable). Similarly, the FDI scheme based on parameter estimation in [11] is promising for passive component degradation, however it does not account for failures in switching components.

In this paper, we present a robust model-based FDI scheme based on linear-switched Luenberger observer for dc-dc power electronic converters. The proposed scheme includes a FD filter and a bank of FI filters. The gain matrix for the FD filter is appropriately designed such that its residual function converges to near-zero in absence of faults and is robust in the presence of noise and other non-idealities. In a fault event, the FD filter residual function exceeds a pre-defined threshold and the bank of FI filters are actuated to determine the faulted component. The bank includes a number of FI filters designed for each converter component, such that the residual function for FI filter which represents the faulted component is minimum of all residual functions generated by other FI filters which represent healthy components.

Both the proposed FDI scheme, and the converter control system are digitally implemented on a single all-programmable system-on-chip (SoC) device. In order to illustrate the performance of the proposed scheme, We present a simulation and experimental validation for a 2 kW dc-dc boost converter used in solar PV applications.

The remainder of the paper is organized as follows. Section II presents the design of the proposed FDI scheme. Section III presents the simulation study. The experimental implementation and results that validate the proposed scheme are presented in Section IV. Section V concludes the paper.

II. Anatomy of Proposed FDI Scheme

In this section, we describe the modeling framework for the dc-dc power electronic converters under nominal and faulted operating conditions, design methodology for the FD and the FI filters, and develop the proposed FDI scheme for a

978-1-5386-1127-2/17/$31.00 ©2017 IEEE

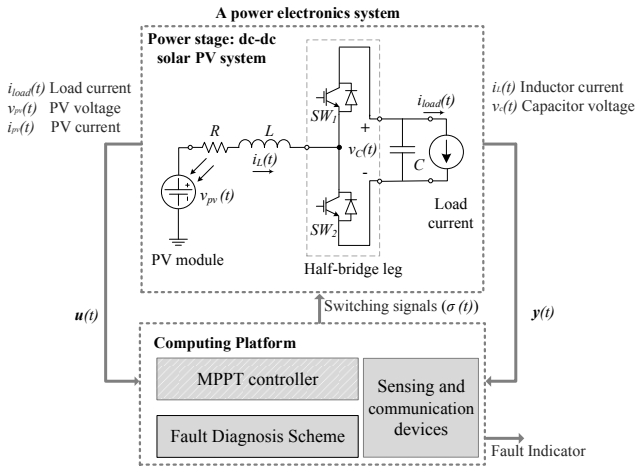

Fig. 1: Implementation strategy for the proposed FDI scheme.

variety of component faults in a dc-dc boost converter. The implementation strategy for the proposed scheme is shown in Fig. 1 for a solar PV power electronic system.

A. Modeling framework for a power electronic converter

The dynamics of a power electronic converter uses a linear-switched model (see [12]). In general, an arbitrary power electronic converter which has piece-wise linear elements can be modeled as :

$$\dot{\mathbf{x}}(t) = \mathbf{A}_{\sigma(t)}\mathbf{x}(t) + \mathbf{B}_{\sigma(t)}\mathbf{u}(t) \quad (1)$$

$$\mathbf{y}(t) = \mathbf{C}\mathbf{x}(t) \quad (2)$$

where $\mathbf{x}(t)$ is the state vector, $\mathbf{y}(t)$ is the output vector, $\mathbf{u}(t)$ is the input vector, $\mathbf{A}_{\sigma(t)}, \mathbf{B}_{\sigma(t)}$, and $\mathbf{C}$ are the collection of linear state space models, and $\sigma(t)$ is the switching signal, which indicates active state space model.

Example 1: Consider a solar photovoltaic power electronic system shown in Fig.1. The linear-switched state-space model of the dc-dc boost converter in the continuous conduction mode is given by :

$$\mathbf{x}(t) = \mathbf{y}(t) = \begin{bmatrix} i_L(t) \\ v_C(t) \end{bmatrix}, \mathbf{u}(t) = \begin{bmatrix} v_{pv}(t) \\ i_{load}(t) \end{bmatrix}, \quad (3)$$

$$\mathbf{A}_{\sigma(t)} = \begin{bmatrix} -\frac{R}{L} & -\frac{s_1}{L} \\ \frac{s_1}{C} & 0 \end{bmatrix}, \mathbf{B}_{\sigma(t)} = \begin{bmatrix} \frac{1}{L} & 0 \\ 0 & -\frac{1}{C} \end{bmatrix}, \mathbf{C} = \begin{bmatrix} 1 & 0 \\ 0 & 1 \end{bmatrix} \quad (4)$$

Table I shows the possible values for the switching signal $\sigma(t)$, where $s_k = 0$ indicates open switch SW_k, and $s_k = 1$ indicates closed switch SW_k, $k \in [1, 2]$.

Next, we model component fault dynamics (e.g. faults in passive and switching elements) in the power electronic converter captured by the state vector in (1) through additive deviations $\Delta\mathbf{A}(t)$ and $\Delta\mathbf{B}(t)$ in the nominal $\mathbf{A}_{\sigma(t)}$ and $\mathbf{B}_{\sigma(t)}$, respectively. Hence, the generalized component fault model is as follows:

$$\dot{\mathbf{x}}(t) = (\mathbf{A}_{\sigma(t)} + \Delta\mathbf{A}(t))\mathbf{x}(t) + (\mathbf{B}_{\sigma(t)} + \Delta\mathbf{B}(t))\mathbf{u}(t) \quad (5)$$

$$\dot{\mathbf{x}}(t) = \mathbf{A}_{\sigma(t)}\mathbf{x}(t) + \mathbf{B}_{\sigma(t)}\mathbf{u}(t) + \mathbf{H}\mathbf{f_i}(t) \quad (6)$$

where $\mathbf{H}$ is an identity matrix; $i = 1, ..., \mathcal{I}$, $\mathcal{I}$ is the number of converter component parameters in the linear-switched state space model; and $\mathbf{f_i}(t)$ is the component fault vector which represents fault severity and a unique direction in fault vector space. Table II represents the components, their parameters and the component fault vectors for common failure modes in the dc-dc boost converter.

TABLE I: Possible open/close switch positions for SW_k

$\sigma(t)$	1	2
s_1	0	1
s_2	1	0

B. Design methodology for FD and FI filters

The proposed FDI scheme includes two classes of fault filters: (1) a FD filter, and (2) a bank of FI filters. The structure of these filters is similar to that of classical Luenberger observer. The design methodology for the FD and the FI filters are described below:

(1) *FD filter:* The linear-switched FD filter is given by following set of equations:

$$\dot{\mathbf{z}}(t) = \mathbf{A}_{\sigma(t)}\mathbf{z}(t) + \mathbf{B}_{\sigma(t)}\mathbf{u}(t) + \mathbf{L}\mathbf{r}(t) \quad (7)$$

$$\mathbf{r}(t) = \mathbf{y}(t) - \mathbf{C}\mathbf{z}(t) \quad (8)$$

where $\mathbf{z}(t)$ is the state estimation vector; $\mathbf{L}$ is the filter gain matrix; and $\mathbf{r}(t)$ is the filter residual vector which is the difference between the measured output $\mathbf{y}(t)$ and the estimated output $\mathbf{C}\mathbf{z}(t)$.

The filter gain $\mathbf{L}$ is computed using linear matrix inequality (LMI) and H_∞ control [13], [14]. Thus, We define an error function $r_e(t)$ given by:

$$r_e(t) = \|\mathbf{r}(t) - \boldsymbol{f}(t))\|_2 \quad (9)$$

where fault vector $\boldsymbol{f}(t) \in \mathcal{F}$ represents an arbitrary fault condition in a converter and a subset of it (i.e. component fault vector) is represented in Table II. The error function $r_e(t)$ satisfies following design objectives: (1) it is asymptotically stable, that is, it converges to zero in both nominal and faulted condition (a common Lyapunov function is chosen to ensure this stability) [13]–[15]; and (2) it satisfies following robust performance condition from $\mathcal{H}_\infty$ control [16]: $\int_0^\infty r_e^T(t) r_e(t) dt < \gamma^2 \int_0^\infty \boldsymbol{f}^T(t)\boldsymbol{f}(t) dt$ where γ is the performance index.

(2) *FI filters:* After a fault is detected, a bank of FI filters is actuated to identify the faulted converter component. Each FI filter in the bank corresponds to a converter component and estimates the related parameter θ_i (see Table II).

Note that We do not precisely estimate a component parameter θ_i. Instead, the conceptual structure similar to that of bang-bang control [17] is used to estimate the parameter at the periphery of its fault boundary (i.e. upper and lower fault bounds of a parameter). The fault boundary defines the allowable fault severity in a component and is set by the user

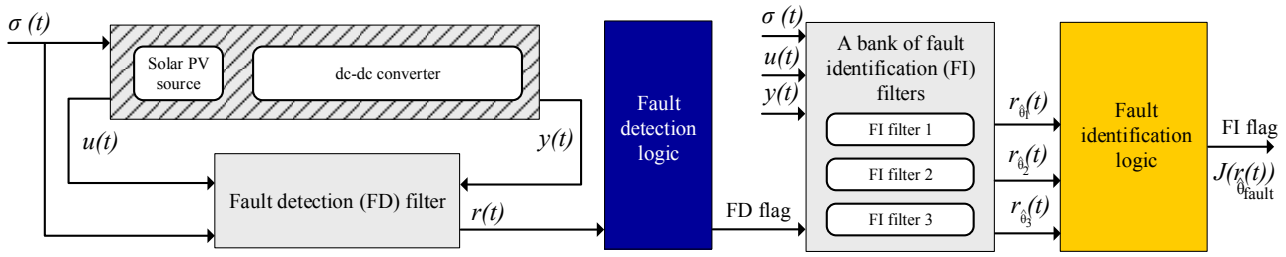

Fig. 2: An overview of the proposed FDI scheme.

TABLE II: Components, their parameters, their common failure modes, and fault vectors (i.e. $\mathbf{f_i}(t)$) for a dc-dc boost converter. A general fault vector $\boldsymbol{f}(t)$ captures the fault dynamics both in magnitude and direction in the fault vector space. Note that $\boldsymbol{f}(t) \in \mathcal{F}$ where $\mathcal{F}$ is the set of all the possible fault vectors in a power electronic converter. For instance, $\mathbf{f_i}(t)$ here represents component fault vectors.

	Component	Parameter	Common failure mode	Fault vector $\mathbf{f_i}(t)$
$i=1$	Capacitor	$\theta_1 = \frac{1}{C}$	Change in capacitance by ΔC	$[0,\ \frac{\Delta C}{C(C+\Delta C)}(i_{load}(t) - s_1 i_L(t))]^T$
$i=2$	Inductor	$\theta_2 = \frac{1}{L}$	Change in inductance by ΔL	$[\frac{\Delta L}{L(L+\Delta L)}(Ri_L(t) + s_1 v_C(t) - \Delta L v_{pv}(t)),\ 0]^T$
$i=3$	Half bridge leg	$\theta_3 = s_1$	Open-circuit fault in SW_2	$[\frac{s_1}{L}v_C(t),\ -\frac{s_1}{C}i_L(t)]^T$
			Short-circuit fault in SW_2	$[\frac{(1-s_1)}{L}v_C(t),\ -\frac{(1-s_1)}{C}i_L(t)]^T$
$i=4$	Series resistor	$\theta_4 = R$	Change in series resistance by ΔR	$[-\frac{\Delta R}{L}i_L(t),\ 0]$

for a FI filter design. This follows from the fact that if power electronic converter is stable during its operation in a fault event, the parameter θ_i will always lie in the certain range $\underline{\theta}_i$ and $\bar{\theta}_i$ where $\underline{\theta}_i$ represents lower fault bound and $\bar{\theta}_i$ represents upper fault bound, that is:

$$\underline{\theta}_i < \theta_i < \bar{\theta}_i,\ \forall\ \underline{\theta}_i > 0,\ \bar{\theta}_i < \infty \tag{10}$$

The linear-switched FI filter for the converter component parameter θ_i is given by following set of equations:

$$\dot{\mathbf{z}}_{\hat{\theta}_i}(t) = \hat{\mathbf{A}}_{(\sigma(t),\hat{\theta}_i)}\mathbf{z}_{\hat{\theta}_i}(t) + \hat{\mathbf{B}}_{(\sigma(t),\hat{\theta}_i)}\mathbf{u}(t) + \mathbf{L}_{\hat{\theta}_i}\mathbf{r}_{\hat{\theta}_i} \tag{11}$$

$$\mathbf{r}_{\hat{\theta}_i} = \mathbf{y}(t) - \mathbf{C}\mathbf{z}_{\hat{\theta}_i}(t) \tag{12}$$

$$\hat{\theta}_i = \underline{\theta}_i + (\bar{\theta}_i - \underline{\theta}_i)\gamma(w) \tag{13}$$

where $\hat{\theta}_i$ is the estimated parameter θ_i in the fault event; $\mathbf{z}_{\hat{\theta}_i}(t)$ is the state estimation vector for $\hat{\theta}_i$; $\hat{\mathbf{A}}_{(\sigma(t),\hat{\theta}_i)}$ and $\hat{\mathbf{B}}_{(\sigma(t),\hat{\theta}_i)}$ are estimates of $\mathbf{A}_{\sigma(t)}$ and $\mathbf{B}_{\sigma(t)}$ for $\hat{\theta}_i$ respectively; $\mathbf{L}_{\hat{\theta}_i}$ is the FI filter gain for $\hat{\theta}_i$; $\mathbf{r}_{\hat{\theta}_i}$ is the corresponding filter residual vector; and $\gamma(w)$ is a binary function which takes value either one or zero to estimate θ_i (see (16)).

The dynamics of FI filter residual $\mathbf{r}_{\hat{\theta}_i}$ for the component parameter θ_i is given by:

$$\dot{\mathbf{r}}_{\hat{\theta}_i} = (\mathbf{A}_{\sigma(t)} - \mathbf{L}_{\hat{\theta}_i}\mathbf{C})\mathbf{r}_{\hat{\theta}_i} + \Psi(\mathbf{z}_{\hat{\theta}_i}(t), \mathbf{u}(t))\delta\theta_i \tag{14}$$

$$\Psi(\mathbf{z}_{\hat{\theta}_i}(t), \mathbf{u}(t))\delta\theta_i = \delta\mathbf{A}_{(\sigma(t),\delta\theta_i)}\dot{\mathbf{z}}_{\hat{\theta}_i}(t) + \delta\mathbf{B}_{(\sigma(t),\delta\theta_i)}\mathbf{u}(t) \tag{15}$$

where $\delta\theta_i = \theta_i - \hat{\theta}_i$, $\delta\mathbf{A}_{(\sigma(t),\delta\theta_i)} = \mathbf{A}_{\sigma(t)} - \hat{\mathbf{A}}_{(\sigma(t),\hat{\theta}_i)}$, and $\delta\mathbf{B}_{(\sigma(t),\delta\theta_i)} = \mathbf{B}_{\sigma(t)} - \hat{\mathbf{B}}_{(\sigma(t),\hat{\theta}_i)}$ respectively. These follow from the fact that $\mathbf{A}_{\sigma(t)}$, $\mathbf{B}_{\sigma(t)}$ and θ_i are not precisely known during a fault in component parameter θ_i.

The FI filter gain $\mathbf{L}_{\hat{\theta}_i}$ is chosen such that (14) under arbitrary switching is asymptotically stable which is determined by a common Lyapunov function $V_{\hat{\theta}_i}(t, \mathbf{r}_{\hat{\theta}_i}) = \mathbf{r}^T_{\hat{\theta}_i}(t)\mathbf{P}_{\hat{\theta}_i}\mathbf{r}_{\hat{\theta}_i}(t)$ where $V_{\hat{\theta}_i} \geq 0$, $\mathbf{P}_{\hat{\theta}_i} > 0$ and $\dot{V}_{\hat{\theta}_i} \leq 0$.

The estimated parameter $\hat{\theta}_i$ is determined by using (10) and (13) where binary function $\gamma(w)$ is defined as [18]:

$$\gamma(w) = \begin{cases} 1, & \text{if } w \geq 0 \\ 0, & \text{if } w < 0 \end{cases} \tag{16}$$

where $w = \mathbf{r}^T_{\hat{\theta}_i}(t)\mathbf{P}_{\hat{\theta}_i}\Psi(\mathbf{z}_{\hat{\theta}_i}(t), \mathbf{u}(t))$.

C. FDI scheme for solar PV power electronic converter

We develop and design the proposed FDI scheme for the solar PV dc-dc boost converter shown in the Fig. 1. The parameters of the dc-dc boost converter for which FD and FI filters are designed are given in Table III. An overview of the proposed FDI scheme is shown in Fig. 2. A FD filter for the proposed system can be described using (7), and (8) where FD filter gain $\mathbf{L}$ is designed using (9).

Fault detection logic: A norm-based residual evaluation function $J(\mathbf{r}(t))$ is generated to make a binary decision on a fault event. The FD filter residual evaluation function is given below [18]:

$$J(\mathbf{r}(t)) = c_1\|\mathbf{r}(t)\|^2 + c_2\int_0^t e^{-\epsilon(t-\tau)}\|^T\mathbf{r}(\tau)\|^2 d\tau \tag{17}$$

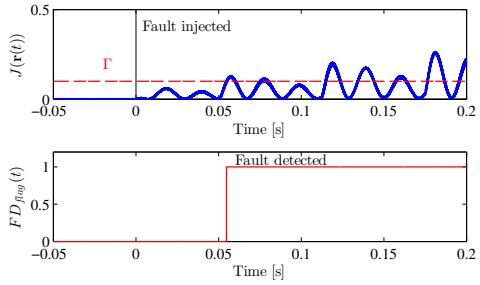

(a) Residual evaluation function $J(\mathbf{r}(t))$ for FD filter (top) and Fault detection logic (bottom).

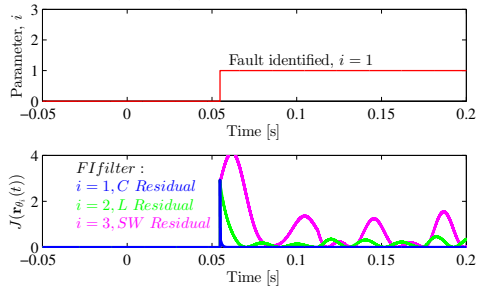

(b) Fault identification logic (top) and FI filter residual evaluation functions $J(\mathbf{r}_{\theta_i}(t))$ where $i \in \{1, 2, 3\}$ (bottom).

Fig. 3: Simulation results for step decrease in capacitance C by ΔC at $t = 0$.

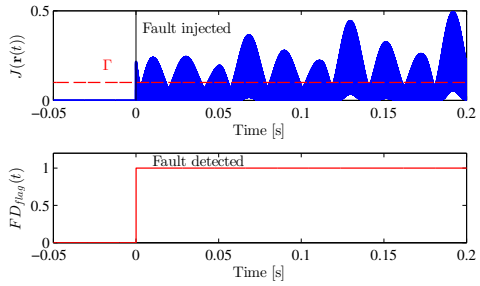

(a) Residual evaluation function $J(\mathbf{r}(t))$ for FD filter (top) and Fault detection logic (bottom).

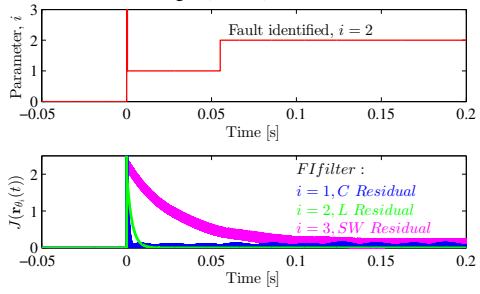

(b) Fault identification logic (top) and FI filter residual evaluation functions $J(\mathbf{r}_{\theta_i}(t))$ where $i \in \{1, 2, 3\}$(bottom).

Fig. 4: Simulation results for step decrease in inductance L by ΔL at $t = 0$.

where $c_1 > 0$ and $c_2 > 0$ are the weighted constants for the instantaneous and past values of L^2 norm of filter residual vector, respectively; and $\epsilon > 0$ is a forgetting factor.

Fault detection is achieved by monitoring the residual evaluation function $J(\mathbf{r}(t))$ at each time step and comparing it with a empirically calculated fault detection threshold Γ as follows: $J(\mathbf{r}(t)) > \Gamma$.

TABLE III: Simulation and experimental parameters

PV emulator ratings	150 V, 40 A, 2 kW
Programmable ac/dc electronic load	300 V, 36 A, 3.3 kW
Boost converter parameters	400 V, 40 A, IGBT devices
L	5 mH $\pm 20\%$
R	1 $\Omega \pm 20\%$
C	2.85 mF $\pm 20\%$
Operating point	
$v_{pv}(t)$	120 V
$v_C(t)$	240 V
$i_{load}(t)$	2 A
Sensing and computing platform	
Model	Xilinx ZynqTM-7000(AP SoC)
Controller time step	500 ns
Switching frequency	10 kHz
Current sensor bandwidth	100 kHz
Voltage sensor bandwidth	100 kHz

Fault identification begins only after a fault is detected. Since fault identification is a classification problem, a template matching algorithm is used. A bank of fault identification filters (which is analogous to a library of fault templates) is designed using (14) and (15) for distinguishing between various component faults $\mathbf{f_i}$, as shown in Table II. Each FI filter can be described using (11), (12), (13), and (16). We design three FI filters for the proposed system which correlates to faults in inductor, capacitor and half bridge leg respectively.

Fault identification logic: It computes the norm-based residual evaluation function $J(\mathbf{r}_{\hat{\theta}_i}(t))$ for each FI filter i in the bank which is given below [18]:

$$J(\mathbf{r}_{\hat{\theta}_i}(t)) = c_{\hat{\theta}_i 1}\|\mathbf{r}_{\hat{\theta}_i}(t)\|^2 + c_{\hat{\theta}_i 2}\int_0^t e^{-\epsilon_{\hat{\theta}_i}(t-\tau)}\|\mathbf{r}_{\hat{\theta}_i}(\tau)\|^2 d\tau \tag{18}$$

where $c_{\hat{\theta}_i 1} > 0$ and $c_{\hat{\theta}_i 2} > 0$ are the weighted constants for the instantaneous and past values of L^2 norm of filter residual vector, respectively; and $\epsilon_{\hat{\theta}_i} > 0$ is a forgetting factor.

Next, the moving window average of each FI filter residual evaluation function is computed. Lastly, the averaged residual evaluation function of all the FI filters are compared with each other to find the minimum of all in the bank, that is:

$$\theta_{fault} = min(\int_{t-W}^{t} J(\mathbf{r}_{\hat{\theta}_1}(\tau))\mathrm{d}\tau, \int_{t-W}^{t} J(\mathbf{r}_{\hat{\theta}_2}(\tau))\mathrm{d}\tau, \int_{t-W}^{t} J(\mathbf{r}_{\hat{\theta}_3}(\tau))\mathrm{d}\tau) \tag{19}$$

where W is the window size for moving average. Note that the residual evaluation function of i^{th} FI filter correlates to a potential fault in i^{th} converter component. Thus, whenever the fault occurs in the corresponding component, the averaged residual evaluation functions of that FI filter converges to a minimum value identifying the faulted component.

III. Simulation Study

Simulation results are presented for detecting and identifying three different kinds of converter component faults which include step decrease in capacitance C by 20% (i.e. Fig. 3),

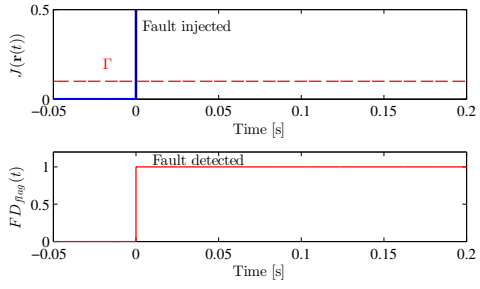

(a) Residual evaluation function $J(\mathbf{r}(t))$ for FD filter (top) and Fault detection logic (bottom).

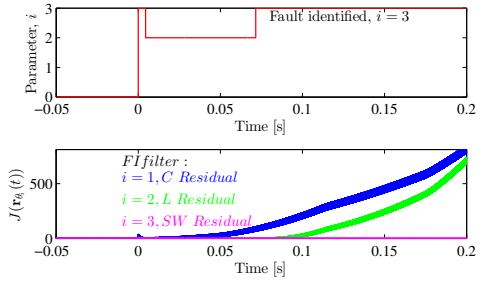

(b) Fault identification logic (top) and FI filter residual evaluation functions $J(\mathbf{r}_{\theta_i}(t))$ where $i \in \{1, 2, 3\}$ (bottom).

Fig. 5: Simulation results for an open switch fault in SW_2 at $t = 0$.

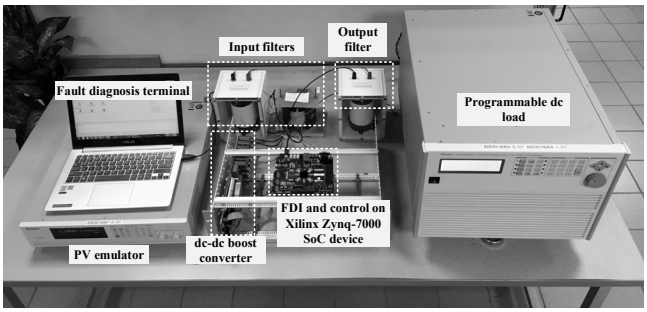

Fig. 6: Validation of the proposed FDI scheme on a prototype solar PV power electronic system.

step decrease in inductance L by 20% (i.e. Fig. 4) and open switch fault in SW_2 (i.e. Fig. 5).

Fig. 3a presents residual evaluation function $J(\mathbf{r}(t))$ for FD filter, which is constantly compared against threshold Γ to detect a fault event. Capacitance fault is injected at $t = 0$ which is detected in 54.7 ms, as shown in fault detection plot. Fig. 3b presents the fault identification logic and the residual evaluation functions for all three FI filters which are computed after the fault is detected. As shown, $J(\mathbf{r}_{\theta_1}(t))$ converges to a minimum value while residual evaluation functions for inductor ($J(\mathbf{r}_{\theta_2}(t))$) and half-bridge leg ($J(\mathbf{r}_{\theta_3}(t))$) struggle to achieve a stable minimum value. To find the minimum residual evaluation function which indicates the faulty element, fault identification logic computes the moving window average of the residual evaluation functions which are compared with each other. The capacitance fault is identified within 54.7 ms.

Similarly, Fig. 4a presents FD filter residual evaluation function $J(\mathbf{r}(t))$ and fault detection logic for inductance fault which is detected in 34 μs. After fault detection, the fault identification logic is activated and the FI filter residual evaluation functions are computed, as shown in Fig. 4b. Since $J(\mathbf{r}_{\theta_2}(t))$ is minimum of all residual evaluation functions (i.e. $J(\mathbf{r}_{\theta_1}(t))$ and $J(\mathbf{r}_{\theta_3}(t))$), fault identification logic correctly identifies it as inductance fault within 55.1 ms.

Lastly, Fig. 5a shows FD filter residual evaluation function $J(\mathbf{r}(t))$ for open switch fault in SW_2 injected at $t = 0$, which is detected in 5 μs. After the fault is detected, fault identification logic computes the residual evaluation functions for the bank of FI filters and identifies open switch fault correctly within 71.6 ms as presented in Fig. 5b.

IV. Experimental Implementation and Results

In this section, experimental implementation details, testbed setup and results are presented for the proposed FDI scheme. The proposed FDI scheme is implemented in FPGA fabric of a single, low-cost all programmable SoC device and experimentally validated on a prototype solar PV power electronic system. The complete specifications of the digital platform and the prototype testbed setup are presented in Table III.

A. Digital implementation of the proposed scheme

The proposed FDI scheme is implemented on an all programmable SoC, a ZedBoard XC7Z020clg484 ZYNQ device. This device combines a dual core ARM Cortex-A9 processor with a field-programmable gate array (FPGA). It enables design flexibility, low latency, and high computation speed, which are necessary attributes for performing FDI and control on power electronic systems. Fault detection and identification filters are discretized and executed with a fixed 500 ns time step on FPGA. Outputs from the PV plant (i.e. V_{pv} and I_{pv}) and the switching power converter (i.e $\mathbf{y}(t)$) are sampled through ADCs using 100 kHz bandwidth sensors for control and fault diagnosis purposes.

B. Solar PV dc-dc boost converter prototype

The programmed SoC device is experimentally tested on a prototype solar PV power electronic system. The complete experimental testbed setup is shown in Fig. 6. It consists of (1) a CHROMA 62150H-600S PV emulator, (2) a dc-dc boost converter, and (3) a programmable dc load. Table III presents additional details of the experimental setup.

C. Experimental results

Experimental results are presented for the proposed FDI scheme which detects and identifies three different kinds of component faults in the dc-dc boost converter (see Fig. 7). These three faults are: (1) step decrease in capacitance C by 66%; (2) step decrease in inductance L by 66%; and (3) open switch fault in IGBT.

Fig. 7a presents fault detection (FD) flag and residual evaluation functions $J(\mathbf{r}_{\theta_i}(t)), \forall\ i \in \{1, 2, 3\}$ where $\mathbf{r}_{\theta_i}(t)$ is generated by i^{th} FI filter in the bank, for capacitance fault. As shown in fault-free condition, both the FD flag and the FI filter residual evaluation functions are zero. When a step decrease in

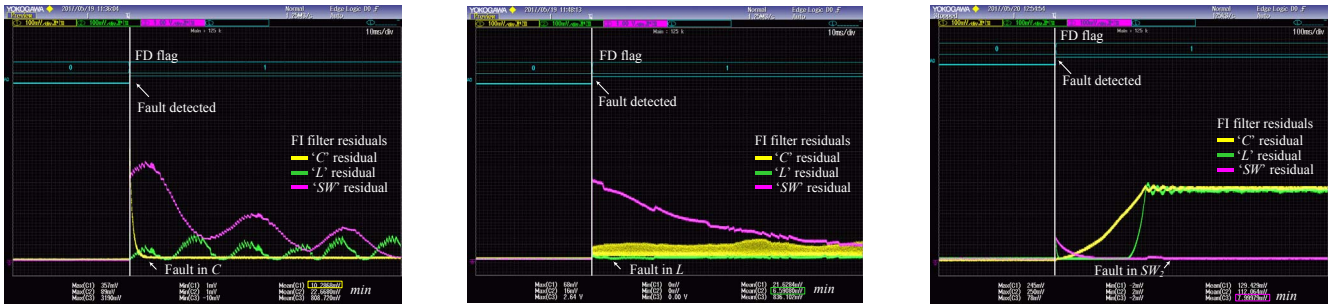

(a) Step decrease in capacitance C by ΔC.

(b) Step decrease in inductance L by ΔL.

(c) Open switch fault in IGBT SW_2.

Fig. 7: Experimental results for proposed FDI scheme.

capacitance value, C is injected, it is detected accurately and the bank of FI filters is actuated to identify the location of fault. The moving average of FI filter residual evaluation function $J(\mathbf{r}_{\theta_1}(t))$ for capacitance achieves the minimum value while those computed for other filters (i.e. $J(\mathbf{r}_{\theta_2}(t))$ for inductor and $J(\mathbf{r}_{\theta_3}(t))$ for half-bridge leg) are always higher.

Similarly, Fig. 7b presents FD flag and residual evaluation functions for all three FI filters when a step decrease in inductance L is injected. The fault event causes FD flag to change from zero to one and actuates the bank of FI filters to determine the faulted component parameter. As shown, the moving average of FI filter residual evaluation function $J(\mathbf{r}_{\theta_2}(t))$ for inductor is minimum of all.

Lastly, FDI of open switch fault in IGBT SW_2 is presented in Fig. 7c where this fault is also detected and identified accurately. As shown, the moving average of FI filter residual evaluation function $J(\mathbf{r}_{\theta_3}(t))$ for half-leg is least of all.

V. Conclusions

This paper presents a FDI scheme for dc power electronic systems which include two new classes of fault filters: (1) a FD filter and (2) a bank of FI filters. Both the FD and the FI filters are based on linear-switched Luenberger observer and are designed analytically using principles of robust and bang-bang control theory. Next, the proposed FDI scheme is developed digitally and implemented on a single, low-cost SoC device. Finally, the scheme is validated on a prototype solar PV power electronic dc system. The experimental results show accurate detection and identification of catastrophic failures in converter components. Furthermore, the proposed scheme could be used to implement fault remediation strategies enabling reliability and fault tolerance into dc power electronic systems.

References

[1] H. Wang, M. Liserre, F. Blaabjerg, P. de Place Rimmen, J. B. Jacobsen, T. Kvisgaard, and J. Landkildehus, "Transitioning to physics-of-failure as a reliability driver in power electronics," *IEEE Journal of Emerging and Selected Topics in Power Electronics*, vol. 2, pp. 97–114, March 2014.

[2] J. Chen and R. Patton, *Robust Model-Based Fault Diagnosis for Dynamic Systems*. Springer Publishing Company, Incorporated, Nov. 2012.

[3] J. Laprie, *Dependability: Basic Concepts and Terminology*. New York, NY: Springer-Verlag, 1991.

[4] J. Poon, P. Jain, I. C. Konstantakopoulos, C. Spanos, S. K. Panda, and S. R. Sanders, "Model-based fault detection and identification for switching power converters," *IEEE Transactions on Power Electronics*, vol. 32, pp. 1419–1430, Feb 2017.

[5] S. Ding, *Model-based fault diagnosis techniques: design schemes, algorithms, and tools*. Springer Science & Business Media, 2008.

[6] M. Shahbazi, E. Jamshidpour, P. Poure, S. Saadate, and M. R. Zolghadri, "Open- and short-circuit switch fault diagnosis for nonisolated DC-DC converters using field programmable gate array," *IEEE Transactions on Industrial Electronics*, vol. 60, pp. 4136–4146, Sept 2013.

[7] E. Ribeiro, A. J. M. Cardoso, and C. Boccaletti, "Open-circuit fault diagnosis in interleaved DC-DC converters," *IEEE Transactions on Power Electronics*, vol. 29, pp. 3091–3102, June 2014.

[8] E. Jamshidpour, P. Poure, and S. Saadate, "Photovoltaic systems reliability improvement by real-time FPGA-based switch failure diagnosis and fault-tolerant DC-DC converter," *IEEE Transactions on Industrial Electronics*, vol. 62, pp. 7247–7255, Nov 2015.

[9] D. R. Espinoza-Trejo, E. Diez, E. Brcenas, C. Verde, G. Espinosa-Prez, and G. Bossio, "Model-based fault detection and isolation in a MPPT boost converter for photovoltaic systems," in *IECON 2016 - 42nd Annual Conference of the IEEE Industrial Electronics Society*, pp. 2189–2194, Oct 2016.

[10] P. Jain, J. X. Xu, S. K. Panda, J. Poon, C. Spanos, and S. R. Sanders, "Fault diagnosis via PV panel-integrated power electronics," in *2016 IEEE 17th Workshop on Control and Modeling for Power Electronics (COMPEL)*, pp. 1–6, June 2016.

[11] J. Poon, P. Jain, C. Spanos, S. K. Panda, and S. R. Sanders, "Fault prognosis for power electronics systems using adaptive parameter identification," *IEEE Transactions on Industry Applications*, vol. PP, no. 99, pp. 1–1, 2017.

[12] J. G. Kassakian, M. Schlecht, and G. C. Verghese, *Principles of Power Electronics*. Addison-Wesley, 1991.

[13] J. L. Wang, G.-H. Yang, and J. Liu, "An LMI approach to H-index and mixed H-/H infinity fault detection observer design," *Automatica*, vol. 43, no. 9, pp. 1656–1665, 2007.

[14] E. Fridman and U. Shaked, "New bounded real lemma representations for time-delay systems and their applications," *IEEE Transactions on Automatic Control*, vol. 46, pp. 1973–1979, Dec 2001.

[15] J. Daafouz, P. Riedinger, and C. Iung, "Stability analysis and control synthesis for switched systems: a switched lyapunov function approach," *IEEE Transactions on Automatic Control*, vol. 47, pp. 1883–1887, Nov 2002.

[16] P. P. Khargonekar and M. A. Rotea, "Mixed H2/H infinity control: a convex optimization approach," *IEEE Transactions on Automatic Control*, vol. 36, pp. 824–837, Jul 1991.

[17] R. Bellman, I. Glicksberg, and O. Gross, "On the bang-bang control problem," *Quarterly of Applied Mathematics*, vol. 14, no. 1, pp. 11–18, 1956.

[18] X.-J. Li and G.-H. Yang, "Fault detection and isolation for uncertain closed-loop systems based on adaptive and switching approaches," *International Journal of Robust and Nonlinear Control*, vol. 26, no. 13, pp. 2916–2937, 2016. rnc.3487.